Citation for published version:
Rizzo, F, Cuomo, S, Pinto, F, Pucillo, G & Meo, M 2019, 'Thermoplastic polyurethane composites for railway applications: experimental and numerical study of hybrid laminates with improved impact resistance', *Journal of Thermoplastic Composite Materials*. https://doi.org/10.1177/0892705719856049

DOI:
10.1177/0892705719856049

Publication date:
2019

Document Version
Peer reviewed version

Link to publication

Rizzo, F. ; Cuomo, S. ; Pinto, F. ; Pucillo, G. ; Meo, M. / Thermoplastic polyurethane composites for railway applications: experimental and numerical study of hybrid laminates with improved impact resistance. In: Journal of Thermoplastic Composite Materials. 2019. (C) The Authors, 2019. Reprinted by permission of SAGE Publications.

University of Bath

General rights
Copyright and moral rights for the publications made accessible in the public portal are retained by the authors and/or other copyright owners and it is a condition of accessing publications that users recognise and abide by the legal requirements associated with these rights.

Take down policy
If you believe that this document breaches copyright please contact us providing details, and we will remove access to the work immediately and investigate your claim.

Download date: 11. Sep. 2019

Thermoplastic polyurethane composites for railways applications: experimental and numerical study of hybrid laminates with improved impact resistance

F. Rizzo[1], S. Cuomo[1], F. Pinto[1]G. Pucillo[2], , M. Meo[1]
[1]Material and Structure Centre, Department of Mechanical Engineering
University of Bath, Bath, UK
[2]Department of Industrial Engineering
University of Naples "Federico II"

Keywords: composite laminate, hybrids, CFRP, TPU, flying ballast, impact energy.

Abstract

Due to the introduction of highly restrictive safety and pollution legislations in the railways industry, weight reduction has become an increasingly important topic over the last decade. Carbon Fibre Reinforced Polymer (CFRP) constitute an excellent alternative to traditional materials, due to their high specific in-plane mechanical properties. Their use in railways industry, however, is currently hindered by their weak out-of-plane properties. Bogies and under-frames are often subjected to impact loadings caused by objects and debris surrounding the tracks (i.e. ice, ballast) that become airborne during the train transit and impact lower-part of the carriage. While metal structures absorb impact energy via plastic deformation, in CFRP Barely Visible Impact Damage (BVID) can occur, weakening the component, and often lead to catastrophic failures.

This work proposes a method for improvement of impact absorption performance of railways composite structures via the addition of a Thermoplastic Polyurethane (TPU) coating to CFRP laminates. The thermo-mechanical behaviour of the thermoplastic layer was investigated Differential Scanning Calorimetry (DSC) and Dynamic Mechanical Analysis (DMA) analyses to optimise the manufacturing process, while damping tests were carried out to demonstrate its unaltered energy absorption ability in the final manufactured structure. TPU/CFRP plates (150 mm x 100 mm of in-plane size) were subjected to 2, 3 and 5J impacts and the results were compared with traditional CFRP laminates. Non-Destructive (i.e. C-Scan, Phased Array) and Compression-After-Impact tests were carried out on the impacted samples to assess the damaged area and residual in-plane mechanical properties. Results show that the TPU layer modifies the energy absorption mechanism, preventing the propagation of damage within the CFRP and resulting in undamaged samples even at the highest energy. In order to predict the TPU/CFRP impact behaviour and identify the best process parameters to optimise impact energy absorption, a Finite Element model was developed and validated using experimental data. The comparison showed good correlation, and a fine approximation of the different impact mechanisms was observed with a maximum error of 5% between experimental and simulated output values. The experimental and numerical results, show that the TPU/CFRP laminates constitute a novel solution for the manufacturing of lighter and safer railways composite structures.

Keywords: Thermoplastic, impact, damage, FEA, TPU

1. Introduction

Over the last twenty years, the mass of rail vehicles has increased by more than 35% due to the technological improvements of structures, subsystems and apparatus necessary to comply with market demands and higher safety requirements (CEN-EN 12663, EN 15227) Indeed, increased comfort requirements pushed manufacturers to install on rail vehicles more complex facilities, such as air conditioning systems, noise and vibration insulations and media devices, in order to improve the quality of the journey. At the same time, as consequence of safety legislation strengthening, railways vehicles became more complex and several mechanical systems, such as brakes and crash boxes, increased their size and weight to satisfy higher performance demands. Heavier trains require greater drive power and therefore railways industry developed larger and heavier motors (electric or diesel) which, in turn, need stiffer and more resistant bogies to withstand stresses caused by larger dynamic solicitations. In addition, higher velocity demanded structural changes in structures such as windows, doors and front cabs, causing an additional weight component for the entire rolling stock due to higher stiffness and more complex geometries necessary to comply with the standards.
All these additional systems and the increased mass of structural component negatively affected the economy of railways industry, leading to a rise in production costs, higher energy consumption, larger amount of CO_2 emissions and greater track wear.

In this context, railway systems require a new technological approach to fabricate light-weight structures for train vehicles, also considering that several railways track providers, such as UK Network Rail, set up their network usage contract charges on the mass of the vehicles to reduce the track consumption and renewal costs (3).
In order to meet the low mass requirement, the use of composites materials in railways structures and components can represent an excellent solution to reduce the global weight of the train structure while keeping the same mechanical properties in terms of stiffness and strength.
In general, major mass distribution in rail vehicles, as stated by Euro Transport Consult (4), is located in motor bogies, motors and drives (22%), car-body (21%), interiors (17%) and trailer bogies (15%). Therefore it is clear that by using composites materials in primary structures, not only it is possible to reduce weight by 20-40% (5) but also lower maintenance costs also due to the higher corrosion resistance typical of composite materials (6,7). Lighter car bodies would also need less power and braking equipment, leading to a reduction of the rotating masses, with an overall mass reduction considering that a traditional high-speed train brake disc weighs around 100 kg (8).

Composite materials in railways have been already used for interiors applications (seats, panels and secondary structures) but only in recent times, some structural applications have been proposed such as a the Glass Fibre Reinforced Polymer (GFRP) bogie realized and tested by Goo et al. under different loading conditions (9), and the front cab sandwich shock absorber designed and simulated numerically by Grasso et al. (10). By applying fibre-reinforced polymers in the primary structures Siemens developed a light-weight train, reducing the mass per seat value by 34% (357 kg) compared to the previous generation trains (4). Heller et al. manufactured a hybrid body railway vehicle using GFRP sandwich composites for both sidewall and ceiling panels, achieving a mass reduction of almost 20% in comparison with a traditional stainless steel body (11). Similarly, CG Rail recently produced a rail vehicle made in large part (around 70%) of composite components, developing a manufacturing process capable of producing large CFRP profiles with wall thickness up to 25 mm. The total mass reduction in comparison with an aluminium car body vehicle is almost 30%, due to a 90% CFRP content in main large structures such as front cab and under-floor panelling (12).

Although the studies mentioned above prove that composite structures are making some headway in the railways industry, one question that still needs to be asked, however, is whether composite components would be able to fully substitute traditional metal structures despite their weak resistance to loads in the out of plane direction. Indeed, it is well known from the aerospace sector that mechanical properties detriment caused by impact events (13) is the principal critical limitation to the implementation of the composites in primary load-bearing structures. Referring to the specific case of railways industry, Onder et al. (14) assessed the damage caused by impact loadings on E-glass/polyester laminate structures and pointed out the effects of impacts at four velocity levels (40 m/s, 70 m/s, 100 m/s, 130 m/s). Goo et al. (9) evaluated the structural integrity of a bogie frame, made of glass/fibre epoxy 4-harness laminate subjected to impacts at three different energy levels (5, 10 and 20 J), showing a detriment of residual properties by almost 18%, with increased damage area at higher energy levels and for sharper edges of the impacting object.

The issue of impact resistance is of fundamental importance for railways components due to flying ballast projections (14), a phenomenon for which general objects such as debris, leaves and ice become airborne due to aerodynamic and mechanical causes, and impact the bottom portion of the vehicle in transit causing damage. These impacts, generally characterised by a minimum energy level of around 5 J (9), can generate Barely Visible Impact Damage (BVID) into composite components, leading to a detriment of mechanical properties in terms of strength and stiffness (15–17) that can

result in unexpected failure of the component, exposing the entire structure and passengers to serious dangers.

Hence, to fully exploit the intrinsic lightness of composite materials within the railways sector, new approaches are constantly investigated to enhance their out-of-plane properties without losing the desired in-plane characteristics. Riccio et al. demonstrated the effectiveness of optimising the laminate layup and skin thickness in order to minimise the delaminated area during composite failure and improve its resistance against out-of-plane dynamic loading (18). In addition, the same authors investigated impact resistance improvement of composite panels via the use of selective stitching to prevent skin-stringer debonding showing superior mechanical properties in comparison with reference (19). Rechack et al. inserted adhesive layers between cross-ply graphite/epoxy laminates and found that the polyamide-epoxy adhesives are able to toughen the interfaces between laminae increasing absorbed energy due to increased contact area (+40%) and reducing matrix cracking (20). Siegfried et al. studied the effect of carbon nanotubes on woven carbonfiber/epoxy composites and evaluated that CNT improved Mode II interlaminar fracture energy (+22% compared with the reference material) and damage tolerance of composite but they also increased their sensitivity to the onset of matrix cracks with a larger delamination area after impact (21). Ruggeri et al. demonstrated a significant increase of impact damage tolerance for composite fan blades applying thermoplastic poluyrethane (TPU) interleave layers, observing no delamination in the interleaved region (22). Following a similar approach, Martone et al. developed a damping behaviour model for thermoplastic polyurethane interleaved composite and reported an improvement in terms of dynamic reponse towards LVI events when the interleave layers are inserted symmetrically within the laminate's stacking sequence (23). Russo et al. instead, proposed a woven glass fibre/thermoplastic polyurethane composite that showed no delamination after impact (even at low temperatures and for thick plates) however, increasing the thickness of the laminates, the effect of the interleaved layers loses its efficiency as an increased crack initiations tendency was recorded (24).

Altough these research works proved the efficiency of the TPU as a energy absorption media for composite materials, the presence of an interleaved layer tends to generate interfacial delamination and debonding issues, with an unacceptable decrement of the in-plane performances. Furthermore, manufacturing processes become more complex with the consequences of extended lamination process time and the necessity of specifically trained operators. In order to overcome these issues, a possible alternative approach is to develop a coating layer that can be laminated on the structure's surface and act as a shielding layer, protecting the laminate thanks to its viscoelastic damping

mechanism and high strain at failure (25) without affecting the in-plane composites properties, while also guaranteeing manufacturing time saving.

Similar solutions are already used in the aerospace industry, where polyurethane coatings are sprayed on the lower areas of aircraft fuselages or used as a protective layer on the landing gear panel against scratches and impact damage caused by landing strip debris (26). Another sprayed coating solution (epoxy resin reinforced with synthetic fibres) is already used in railways in order to protect bogie axles from any debris or objects and any corrosion phenomena (27). However, all these applications require skilled operators to carry out the coating operations, giving restrictive limits in terms of manufacturing and increasing the cost of the final product.

In this work, a TPU layer was introduced as a superficial layer on the impact surface of CFRP laminates to improve impact performances. A "one-step" manufacturing solution is proposed to carry out the coating operation at the same time of the consolidation of the CFRP laminae in autoclave without any added complexity to the manufacturing process.

Prior to the experimental campaign, an extensive material charachterization for TPU material was carried out in order to verify its compatibility with the autoclave curing process and in particular to avoid any degradation or reaction with the composite's matrix at high temperatures. Differential Scanning Calorimetry (DSC) and Dynamic Mechanical Analysis (DMA) were carried out to determine the variation of the TPU's mechanical behaviour and its suitability for autoclave uses during both cooling and heating processes and under mechanical loads at different frequencies.

Once the TPU compatibility for autoclave process was verified, the effectiveness of the coating as protective layer was investigated, via extimating the damping ability of the TPU by measuring the vibrations suppression characteristics of the coated and uncoated laminates. In order to measure the improvement in the out-of-plane properties, an experimental campaign was carried by subjecting TPU-coated CFRP panels to Low Velocity Impacts (LVIs) and comparing the results with traditional CFRP laminates. Three different energy levels, 2 J, 3 J and 5 J to simulate the BVID inflicted by flying ballast and damaged areas were analyzed using non-destructive damage detection techniques (C Scan – Phased Array and CT-Scan). In order to have a deeper understanding of the phenomena involved during the impact event and to offer a cost-effective support for the future design of commercial products using TPU/CFRP composite as structural material, a 3D Finite Element Analysis (FEA) model was developed using an explicit LS-DYNA software (R10) and validated using impact data."

Furthemore, using a Compression-After-Impact (CAI) test, residual mechanical properties of the impacted samples were investigated and correlated with the damaged area evaluation.

1.1. Thermoplastic Polyurethane

TPU is a polymer formed by linear segmented block copolymers having soft amorphous segments and hard crystalline segments (28). Soft segments are made of long flexible polyether or polyester chains while hard segments are made of diisocynate with the addition of a chain extender (low molecular weight diol). In the polymer meso-structure, each soft segment is linked to two hard ones which are interconnected by hydrogen bonds and act as multifunctional tie points, creating a physical crosslink and reinforcing fillers. On the other hand, soft segments generate an elastomers matrix, which is responsible for the TPU elastic properties. This polymeric blend is used in several engineering applications due to its mechanical strength, low-temperature high performance and impact energy absorption and therefore it was selected as protective layer for this experimental work.

2. Material Characterization

In order to evaluate the physical and chemical properties of the TPU and its manufacturing behaviour when used as a coating on a CFRP structure, an extensive characterization campaign was carried out. In this experimental part, the thermo-mechanical behaviour of TPU was analysed using DSC and DMA in order to evaluate the TPU suitability of autoclave assisted cure procedures. DSC was used to evaluate the thermal parameters of the thermoplastic polymer such as Glass Transition (Tg) and Melting point (Tm), fundamental for composite-TPU cure process optimisation. DMA, instead, was carried out to confirm the invariance of the TPU mechanical behaviour at different temperatures (-50 / +180 °C) and frequencies to verify compliance with the typical railways operative conditions.

2.1. DSC – Differential Scanning Calorimetry

A DSC Q20 (TA Instruments, New Castle,USA) was used to operate the thermal tests. Four tests were carried out on samples weighting 6-8 mg and following the same temperature programme cycle: 1) heating – 2) cooling – 3) heating. Three tests reached the maximum temperature of 170 °C while the last test was heated up to 200 °C, to investigate the presence of any melting process also at temperatures above the traditional curing temperature of carbon laminates.

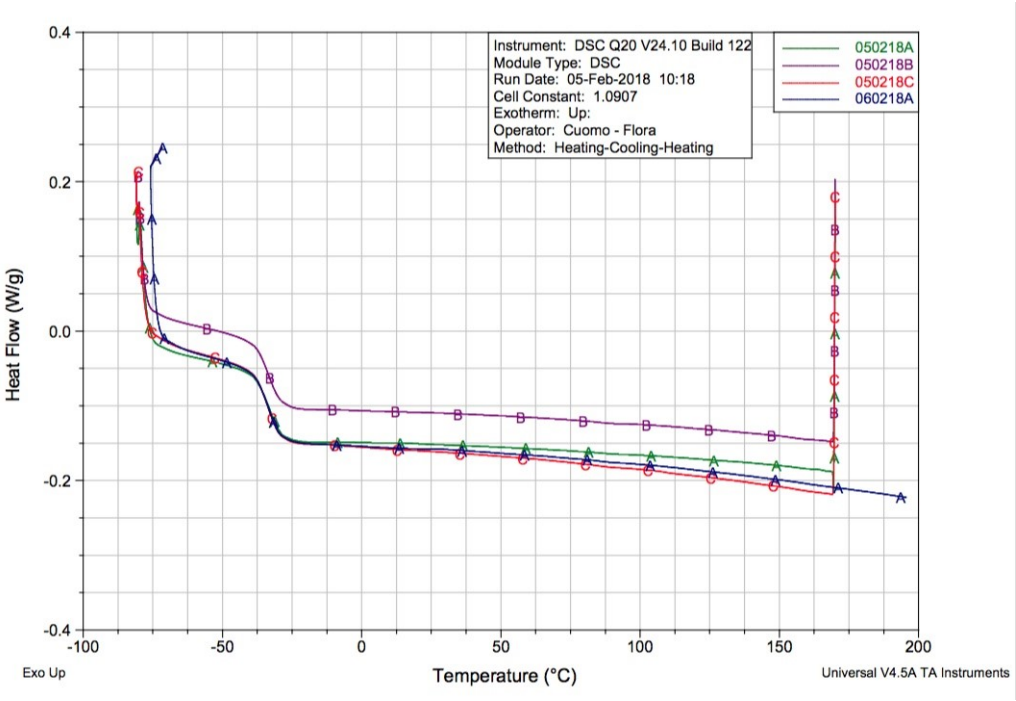

Figure 1. Temperature vs Heat Flow curves obtained for the different TPU samples

In Figure 1, DSC curves clearly show an average glass transition at -33.35°C, demonstrating that TPU is suitable for railways applications also in climatic areas where extreme temperatures conditions are reached during winter, without any risk of transition from the rubbery to the glassy state, hence without damping performances detriment.

In addition, no melting process (absence of endothermic peak) is highlighted, even in the last run (060218A curve in Figure 1) at 200°C. Considering that melting is a typical phenomenon of the crystalline domains, this behaviour suggested that the TPU selected for this experimental campaign was completely amorphous and suitable for its use at high temperature.

2.2. DMA – Dynamical Mechanical Analysis

To evaluate material response variation toward load frequency and temperature, a Tritec 2000 DMA (Tryton Technology Ltd., Leicester, UK) was used to perform Tensile/Temperature and Tensile/Temperature/Frequency scans, following the ISO 6721-11:2012 standard (29). Both these tests are necessary since in a complex system like a rail vehicle, sudden temperature changes can affect the mechanical response of specific components and possible defects in the primary structures can generate vibrations in a frequency range usually between 1 and 50 Hz. Indeed, it is worth noting that a damaged wheel running at 250 km/h with a radius of 0.5 meters, is able to generate an excitation with a frequency of 22 Hz that directly affects the railway car body.

In Temperature-scan the specimen was subjected to an oscillating stress, varying the temperature from -60 to 180 °C, with two frequencies (1-10 Hz) and a heat rate of 2 °C/min. In Frequency-scan, the max temperature was set at 100 °C, the heat rate at 2 °C/min and the frequency varied between 1 and 80 Hz. Liquid nitrogen was used as cooling medium during both tests.

It is important to underline that the setup parameters were chosen considering the operative limits of railways defined by legislation (1-50 Hz in frequency and -25 /+45 °C as third climatic class temperature range –EN 50125.2008), able to verify the suitability of TPU in this application.

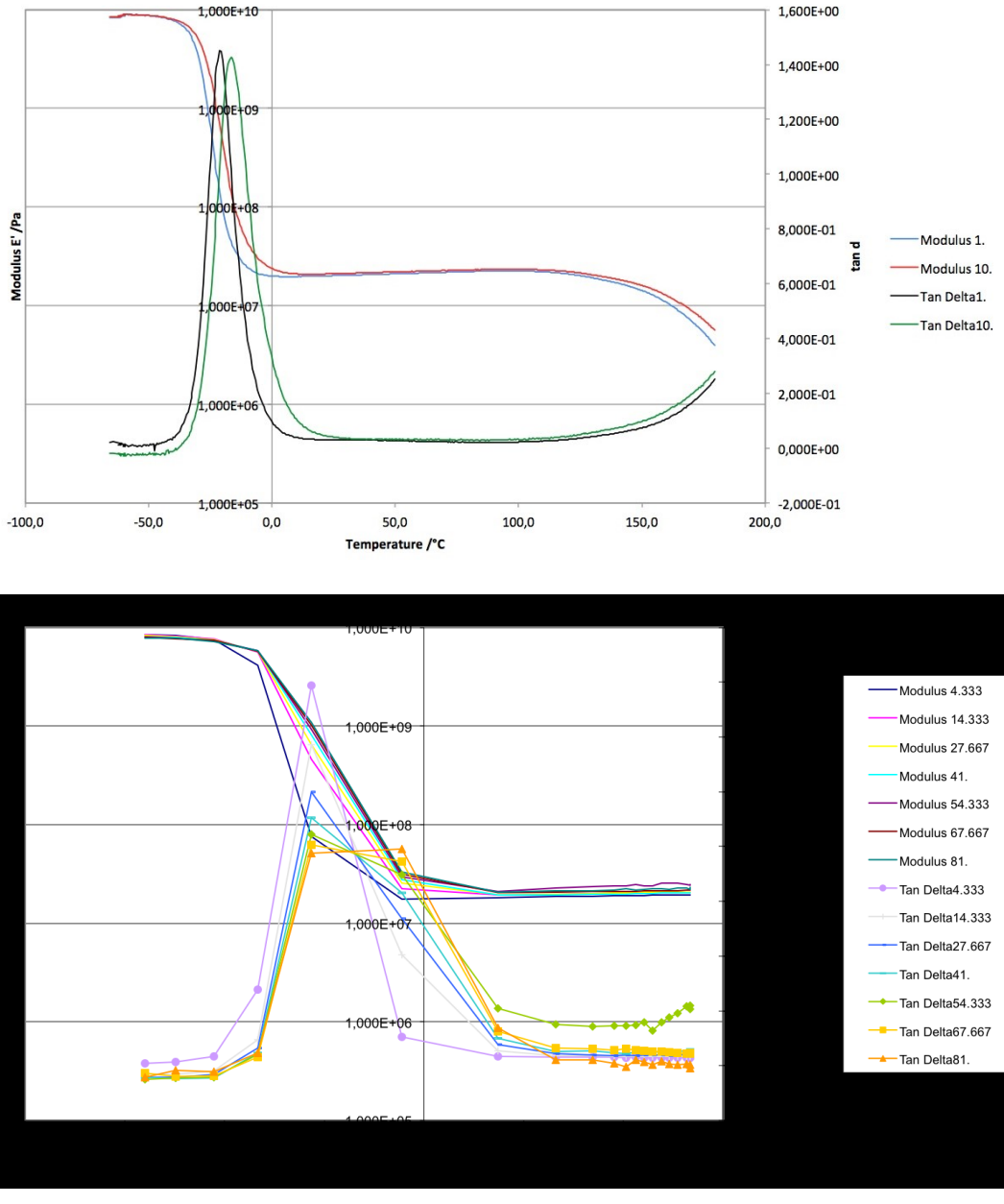

Figure 2. Temperature Scan (top) Frequency Scan (bottom)

Figure 2 shows the characteristic trend of the storage modulus E' and the damping tan δ varying with temperature and frequency. For very low temperatures, since molecular chains are tight and fixed, no

responses are allowed to the applied stress and there is no resonance with the sinusoidal load, due to high stiffness (glass state). As heating increases, glass transition occurs and the chains in the amorphous region start a large-scale motion, resonating with the applied load. In this phase, the storage modulus decreases by one order of magnitude and the molecular motion associated with the glass transition is time dependent. Therefore, Tg increases when heating rate increases or test frequency increases; hence, output data showed above are consistent since in the glass transition range, both tan δ peak and storage modulus variation, are shifted to higher temperatures as the frequency is increased from 1 to 10 Hz Figure 2 top) and from 1 to 80 Hz (Figure 2 bottom). After glass transition, it is possible to evaluate a rubbery plateau due to the slippage of the molecular chains. When the temperature reaches the onset melting, free volume increases and the material is able to flow since the molecular chains can slide on each other. Analysing the results it is also clear that after 150 °C the material starts showing signs of degradation of mechanical properties, compromising the dynamical response of the material, which becomes frequency dependent. From the Frequency scan (Figure 2 bottom) it is pointed out that, at different railways operative frequencies, TPU undergoes a variation of Tg from -30 °C to -20 °C, but considering that this value is still way below operative conditions, this means that even in harsh winter environments TPU will show no changes in terms of damping ability and elastic properties.

Based on these results, it is possible to conclude that the use of TPU is suitable for railways applications where a broad range of different frequencies excitations affect the vehicle and his structures. However, considering that the molecular structure of the TPU will start to degrade at 150°C and that the cure temperature for epoxy systems used in this study is 180°C, it would not be possible to include the TPU layer with the uncured CFRP layers in a “one-step” manufacturing procedure. To address this, a reduction of curing temperature, with a consequent increase of curing time, is necessary to guarantee the correct and complete cure of the CFRP laminate and the stability of the TPU polymeric system. The new cure time was obtained using a numerical linear interpolation (Figure 3) considering the starting temperature (180°C) and time (3h) parameters and fixing the final temperature (120°C).

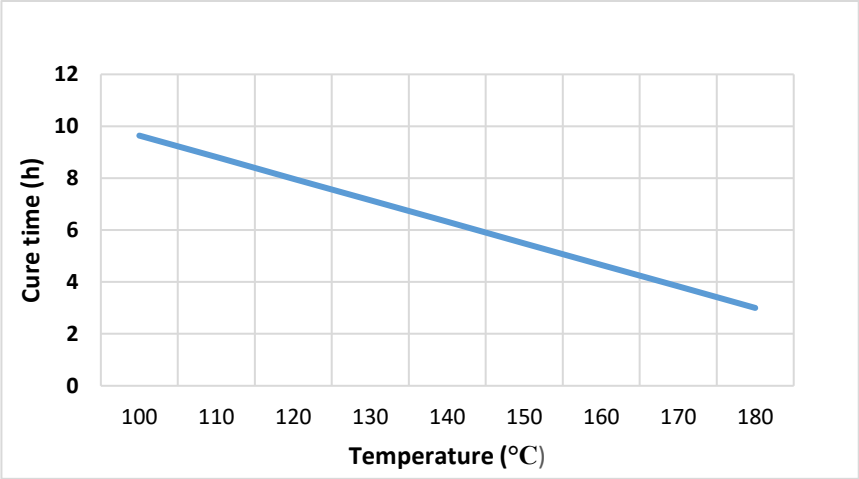

Figure 3-Interpolation curve used to estimate the cure time of the TPU-coated samples.

2.3. Damping Test

To evaluate the energy absorption properties of TPU/CFRP samples, damping tests were carried out. The test configuration (Figure 4) was a single cantilever beam (80 mm x 10 mm; w/l=1/8), excited with an impulsive load on the free end and the oscillations were measured by a laser transducer (μ ε optoNCD T2300).

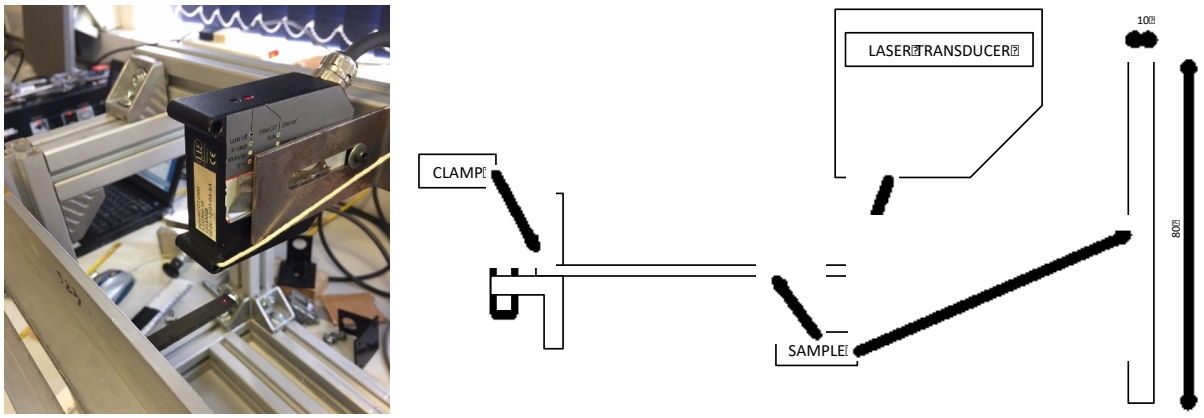

Figure 4-Damping test setup (left) and scheme (right).

The capability of the TPU/CFRP samples to attenuate the impulsive load was evaluated with the logarithmic decrement δ_{av}, which can be defined as:

$$\delta_{av} = \frac{1}{n}\ln\left(\frac{U_{n-1}}{U_n}\right) \quad (1)$$

where U_n is the amplitude of the oscillation.

In order to evaluate the optimal damping performances, different configurations of TPU/CFRP samples were tested.

The main configuration was obtained following the one-step manufacturing process, with TPU applied simultaneously with uncured CFRP (TPU Autoclave Cured) and the results were compared with an uncoated laminate (Autoclave Cured). Moreover, in order to analyse the effectiveness of the proposed manufacturing process, damping tests were performed also on another configuration where the TPU layer was applied on the surface of an already cured laminate using a traditional epoxy adhesive (TPU Glued).

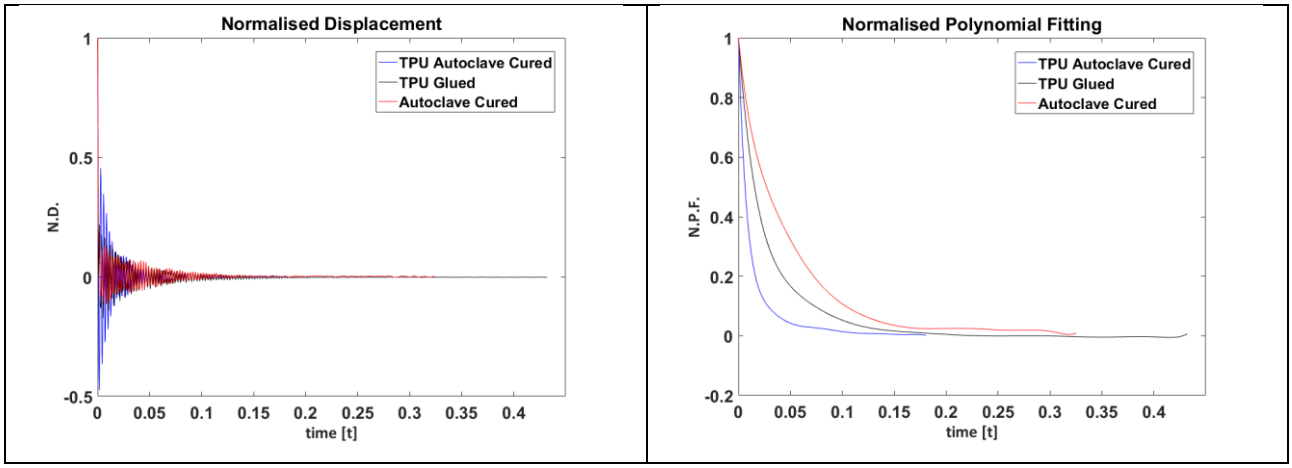

Figure 5- Damping test results: Displacement (left) and Damping (right) Curves

% variation compared to the reference (N_x)						
Type	**δ_av**	**Variation**	**Weight [g]**	**Variation**	**δ per unit of weight**	**Variation**
Autoclave Cured	0,0557	/	2.505	/	0.0222	/
TPU Glued	0,1014	182%	3.43	+36.9%	0.0300	135%
TPU Autoclave Cured	0,2160	387%	3.378	+34.8%	0.0629	283%

Table 1- Logarithmic decrement (δ_{av}) and weight variations for TPU Autoclave Cured and TPU Glued configurations compared to Autoclave Cured (control).

Analysing the logarithmic decrement evaluated for the different configurations (Figure 5), the TPU in the CFRP laminate leads to an increase of damping properties in both one-step and glued manufacturing procedures, showing an increase of 387% and 182% respectively, in comparison with traditional CFRP laminates. It is important to underline, however, that the presence of the TPU layer affects the weight of the laminate, therefore these results were rescaled evaluating the values of δ per unit weight (see Table 1), leading to a variation of +283% and +135% for the two configurations.
In conclusion, considering the significant increment in damping properties for the "one-step" manufacturing procedure, this configuration was selected for the impact test sample manufacturing.

2.4. Samples Manufacturing

The material used to fabricate the CFRP samples was a carbon fibres pre-preg (CYCOM 977-2 thermoset epoxy system). A cross ply staking sequence of 11 plies ($[0/90/0/90/0/\overline{90}]_s$) was used during the layup procedure where each ply was cut at 150 mm x 100 mm in size. Prior to the autoclave process, the uncured CFRP was coated via direct application of the TPU layer and a metal plate was used as mould to obtain a good adhesion between the two materials. Images of the manufactured samples are reported in Figure 6.

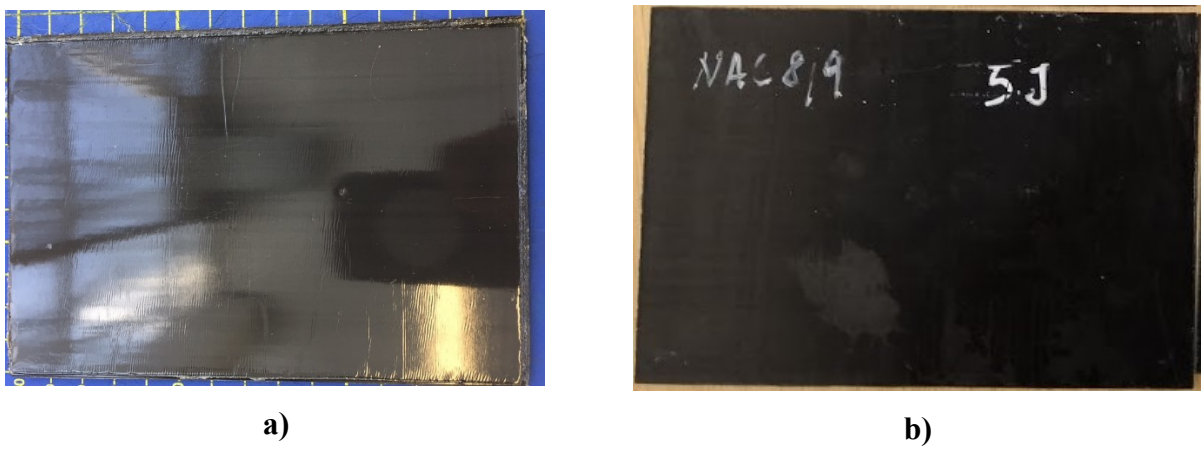

a) **b)**

Figure 6-Standard impact plates used during experimental campaign: a) TPU-coated CFRP and b) traditional CFRP

The average thickness of the laminates was 2.00 mm (CFRP) and 2.8 mm (TPU/CFRP). A sketch of the sample layup is reported in Figure 7.

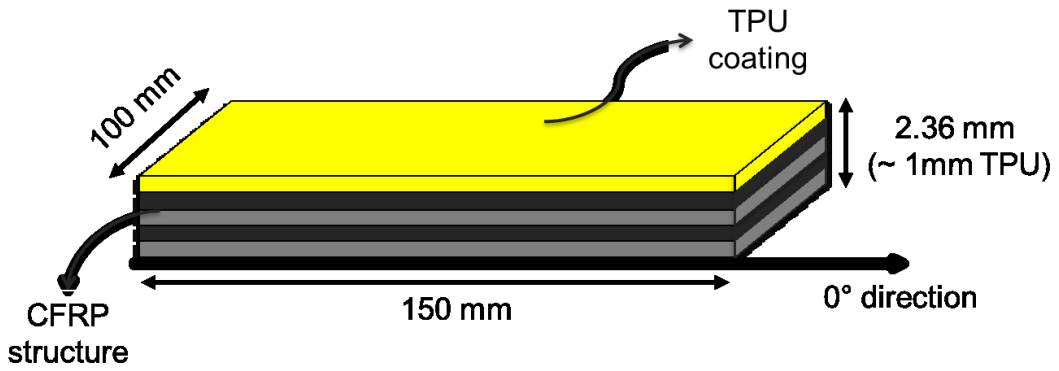

Figure 7- Sketch of TPU-coated CFRP plates used during impact campaign

3. Low Velocity Impact Test

3.1. Experimental setup – LVI tests

Impact tests were carried out on TPU/CFRP samples and compared with traditional laminates to investigate the effects of the TPU layer on the impact properties of the composite structure. Three

different energy levels (2J, 3J and 5J) were used to simulate the minimum conditions to generate a flying ballast BVID in a CFRP structure as specified by the European Regulatory Framework. The samples were placed into the impact machine (2.66 kg shuttle weight) using a dedicated clamping support to apply the appropriate boundary conditions in order to avoid undesired vibrations.

Impact data were collected using a Kistler Accelerometer and raw signals (Time-Volt) were converted into Force-Displacement curves following BS EN ISO6603-1:2000 and BS EN ISO6603-2:2001 standards. The impactor rig scheme and apparatus are illustrated in Figure 8. All the samples were impacted following the same procedure with TPU samples being impacted with the polymer layer facing the impactor tip.

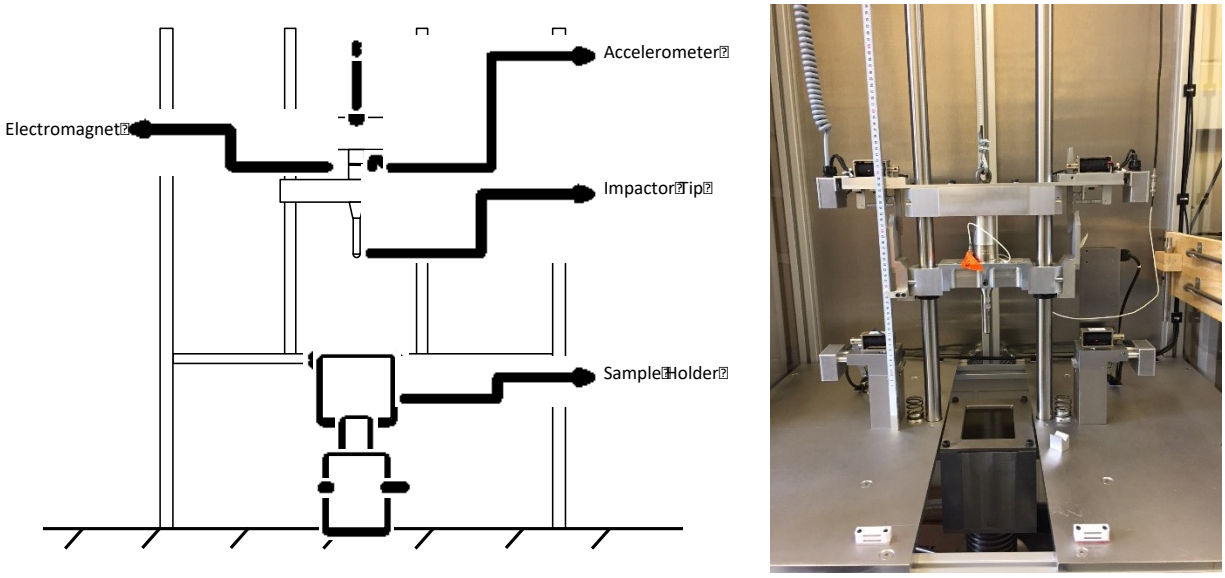

Figure 8-Impactor Rig scheme and detail

3.2. Experimental setup – Phased-Array scan and CT scan

The planar extension (2D) of the internal damage was investigated using a 5MHz Phased-Array Transducer at 128 Channels (National Instrument, Austin, CA). The beam length of each transducer corresponds to 0.58 mm in the real scale of the sample and the images were collected with a fixed width size of 225 pixels. A digital-real scale conversion was, then, possible through direct correlation between the full length of 128 transducers (real dimension) and the relative pixels collected (digital). Images displayed the in-plane amplitude variation in a 16-bit colour-map scale from which damaged areas can be identified. The colour scale used was between 0 and 40 V where the colour red was the maximum value and the colour white the minimum.

Volumetric (3D) images of internal damaged areas were collected using a Computed Tomography (CT) Scan (Nikon XT H 225, Tokyo, Japan) to confirm the results obtained with the Phased-Array and to further analyse the impact damage typology in three dimensions. Images were collected for the entire volume of the samples and then elaborated to show the fit view of the damaged areas.

3.3. Experimental setup – Numerical model

The testing required for the validation of a specific design in terms of safety and reliability is both expensive and time consuming due to the entity and complexity of the process also due to the wide range of design parameters that need to be taken into account during the development of new material solutions to manufacture primary structural components.

Finite Element (FE) modelling is one of the most powerful tools used by modern industry to reduce the number of experimental tests that are required to validate a certain design, leading to a consequent reduction in costs and process time. Indeed, after its validation, the use of numerical model allows to optimise critical design parameters (weight, size and geometry) that advanced sectors demand for the application of TPU/CFRP. Based on this premise and on the necessity to develop an accurate design and an optimisation tool for a future use of TPU/CFRP laminates in real commercial parts, a three dimensional (3D) explicit Finite Element Model (FEM) was implemented using LS-DYNA. The computational FE mesh is reported in Figure 9 where in the side view, it is possible to see the presence of TPU (top layer) as coating for the CFRP laminate.

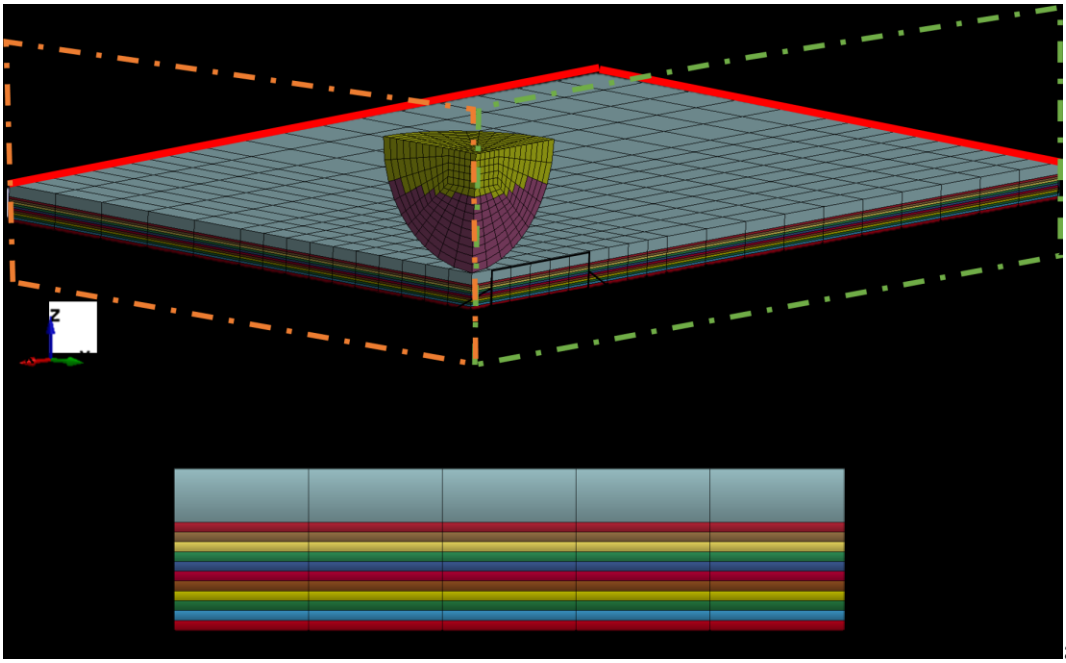

a)

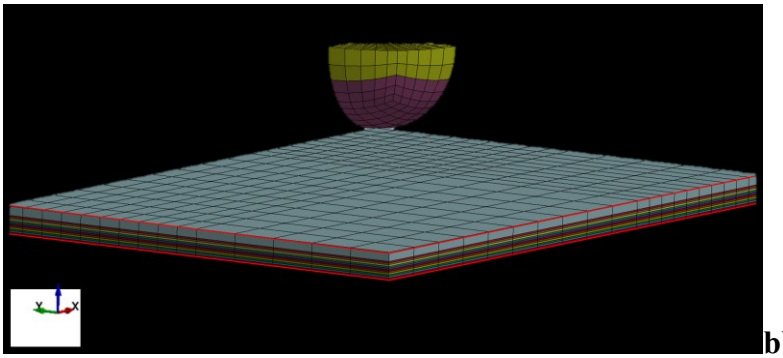

b)

Figure 9-FE mesh used in the simulated LVI: a) front-isometric and lateral view with detail of the TPU coating and CFRP plate where symmetric planes and boundary conditions are reported and b) back-isometric view of the boundary conditions of the plate

The impactor body was simulated as a hemispherical body of 20 mm diameter, a mass of 2.66 kg and 3D brick elements using an ELASTIC isotropic material card (E=210 GPa and ν=0.3). The material was assumed elastic (no plastic deformation) since impact velocity is very low (1.93m/s for 5J case) and no plastic deformation was observed on the impacting tip during the experimental case. Parameters used during the analyses are reported in Table 2.

MATERIAL	RO (Kg/m^3)	E11 (GPa)	E22 (GPa)	E33 (GPa)	PR21	PR31	PR32	G12 (GPa)	G23 (GPa)	G31 (GPa)	X1t (MPa)	X1c (MPa)
CFRP	1530	110	4.9	4.9	0.0535	0.0535	0.449	4	4	4	1500	950
MATERIAL	X2t (MPa)	X2c (MPa)	S12 (MPa)	S23 (MPa)	S31 (MPa)	ENKINK (J/m^2)	ENA (J/m^2)	ENB (J/m^2)	ENT (J/m^2)	ENL (J/m^2)		
CFRP	70	200	80	80	80	75100	50100	478	900	900		

Table 2-MAT_261 orthotropic material card paramters:RO: density, modulus of elasticity (E11, E22, E33), poisson's ratios (PR12 ,PR31, PR32), shear modulus (G12, G23, G31), normal and transverse strenght under traction and compression (X1t, X1c, X2t, X2c), shear strenght (S12, S23, S31), compresisve fibre failure energy (ENKINK), tensile fibre failure energy (ENA), Intralaminar matrix tensile energy failure (ENB), Intralaminar matrix trasnverse shear energy failure (ENT) and Intralaminar matrix longitudinal shear energy failure (ENL).

A constant stress element formulation was used to model the 3D brick elements with an average in-plane size of 2.5mm. Each ply was modelled using a single 0.18mm thick element layer. The material characteristics of the composite plate (150 mm x100 mm x 3 mm in size) was defined using a MAT_261 (LAMINATED_FRACTURE_DAIMLER_PINHO) orthotropic material implementing a progressive damage model considering non-linear in-plane shear behaviour (32). The definition of angles and stresses in fracture plane are reported in Figure 10

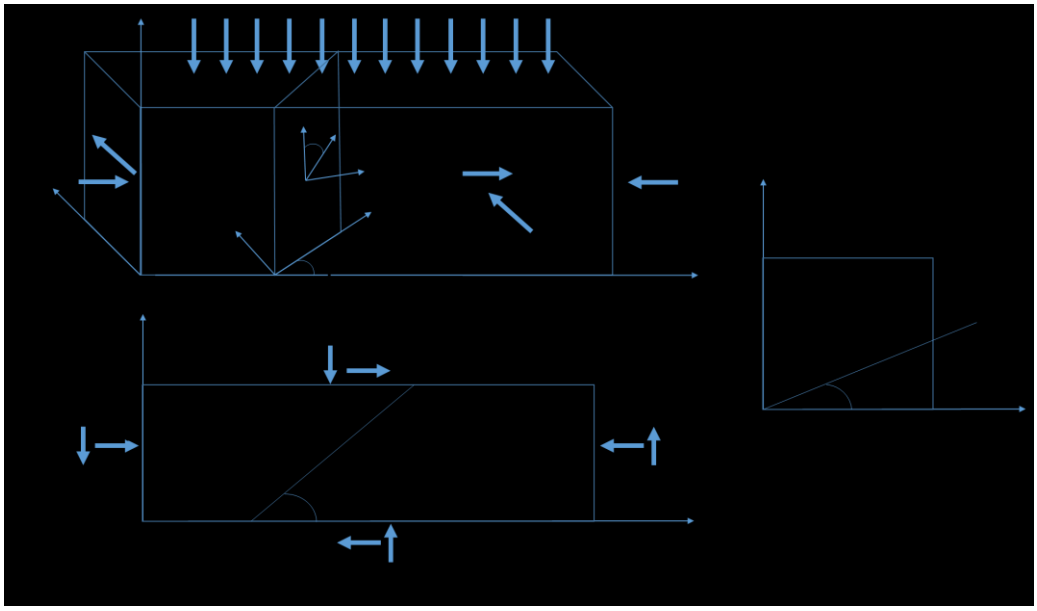

372 **Figure 10- In fracture plane stresses and angles definition (29)**

373

374 The damage initiation for longitudinal and intralaminar failure was calculated using the stress state
375 for each time step and the relative material strength parameters. Failure criteria are defined as:

Logitudinal (fiber) tension

$$\frac{\sigma_a}{X_{1t}} = 1 \qquad 2)$$

Longitudinal (matrix) failure:transverse tension (if σ_n>0)

$$\left(\frac{\sigma_n}{X_{2t}}\right)^2 + \left(\frac{\tau_T}{S_T}\right)^2 + \left(\frac{\tau_L}{S_{12}}\right)^2 = 1 \qquad 3)$$

Longitudinal (matrix) failure:transverse compression/shear (if σ_n<0)

$$\left(\frac{\tau_T}{S_T - \mu_T \sigma_n}\right)^2 + \left(\frac{\tau_L}{S_L - \mu_L \sigma_n}\right)^2 = 1 \qquad 4)$$

With

$$\begin{aligned}
\sigma_n &= \frac{\sigma_b + \sigma_c}{2} + \frac{\sigma_b - \sigma_c}{2}\cos(2\Phi) + \tau_{bc}\sin(2\Phi) \\
\tau_T &= -\frac{\sigma_b - \sigma_c}{2}\sin(2\Phi) + \tau_{bc}\cos(2\Phi) \\
\tau_L &= \tau_{ab}\cos(\Phi) + \tau_{ca}\sin(\Phi) \\
S_T &= \frac{X_{2c}}{2\tan(\Phi_0)} \\
\mu_T &= -\frac{1}{\tan(2\Phi_0)} \\
\mu_L &= -S_{12}\frac{\mu_T}{S_T}
\end{aligned} \qquad 5)$$

$$\mu_L = -S_{12}\frac{\mu_T}{S_T}$$

considering Φ_0 as the fracture angle (53°). Longitudinal compression failure criterion definition can be found in literature (29). In Figure 11, the damage evolution law for MAT_261 is reported for each failure criterion.

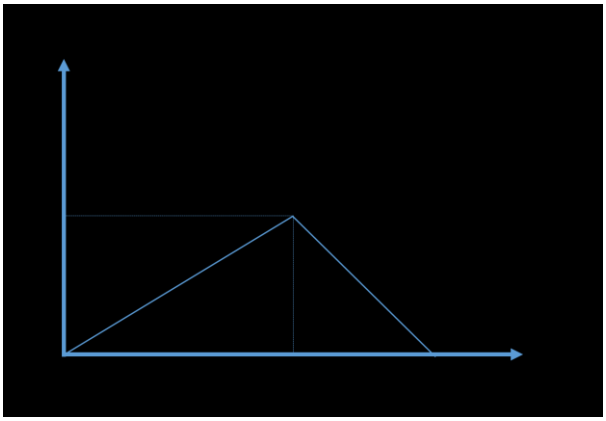

Figure 11-damage evolution law for MAT_261 (29)

When the stress state is within the criteria values, the material behaves as elastic orthotropic. When, instead, one of the criteria is met, the stress is reduced by a coefficient of *(1-d_j)* where d_j is one of the damage function of the different failure modes, showing a fracture-based linear damage evolution with fracture toughness (one for each failure criterion) as critical value (C). Each damage function is normalised for the element characteristic length X (see Figure 11) to have consistency between different element sizes. Element erosion was, then, evaluated for each element that satisfies one of these fracture criteria. All the equations on damage initiation and fracture criteria were reported in the MAT_261 card section of the material manual (33). In order to predict the delamination component during the dynamic event and take into account the interlaminar properties of laminated material, a TIEBREAK_CONTACT (OPTION 6) was implemented between each layer of the hybrid structure. This particular contact (34) couples together the nodes of two adjacent plies until failure initiation, defined by interlaminar interface toughness G_{IC} (230 J/m^2) and G_{IIC} (650 J/m^2) and the relative normal ($\sigma_f = 4.6MPa$) and shear ($\tau_f = 13MPa$) stresses. The tiebreak failure criterion is defined using the normal and shear components of the stress state at a certain time step:

$$\left(\frac{|\sigma_n|}{\sigma_f}\right)^2 + \left(\frac{|\tau_n|}{\tau_f}\right)^2 \geq 1$$

Where σ_n and τ_n are the normal and shear stress."

Afterward the damage was scaled in function of the inter-laminar distance until complete interface separation that occurs when the distance between the plies reaches its critical value (0.1mm).

Then, the contact is converted into a traditional PENALTY_BASED contact. The. TPU coating material was simulated using an isotropic VISCOELASTIC material card (35,36) and all the used elastic parameters were defined considering the results obtained from DMA tests and data fitting with experimental results. The viscoelastic material properties are defined by the equation 7:

$$G(t) = G_\infty + (G_0 - G_\infty)e^{-\beta t} \quad (7)$$

where G_0 represents the short-time shear modulus (~6.4GPa), G_∞ the long-time shear modulus (4.4GPa), β the decay constant (~1) and t the time of observation. This material was chosen since no relevant permanent deformation are found on the real TPU layer after the impact event and therefore the viscoelastic behaviour for the involved impact energies can be assumed without plastic effects. Boundary conditions of mesh model are applied by constraining all displacements along the z-direction of the external lateral edges of the plate. Interaction between impactor body and TPU/CFRP surfaces is modelled using PENALTY_BASED contact for which the erosion of elements with negative volume is allowed to avoid numerical issues. All the materials parameters used in the numerical model are reported in Table 2.

3.4. Results and Discussion

Output data obtained from the impact campaign are reported in Figure 10 in which Force-Time and Force-Displacement curves and their comparison are illustrated.

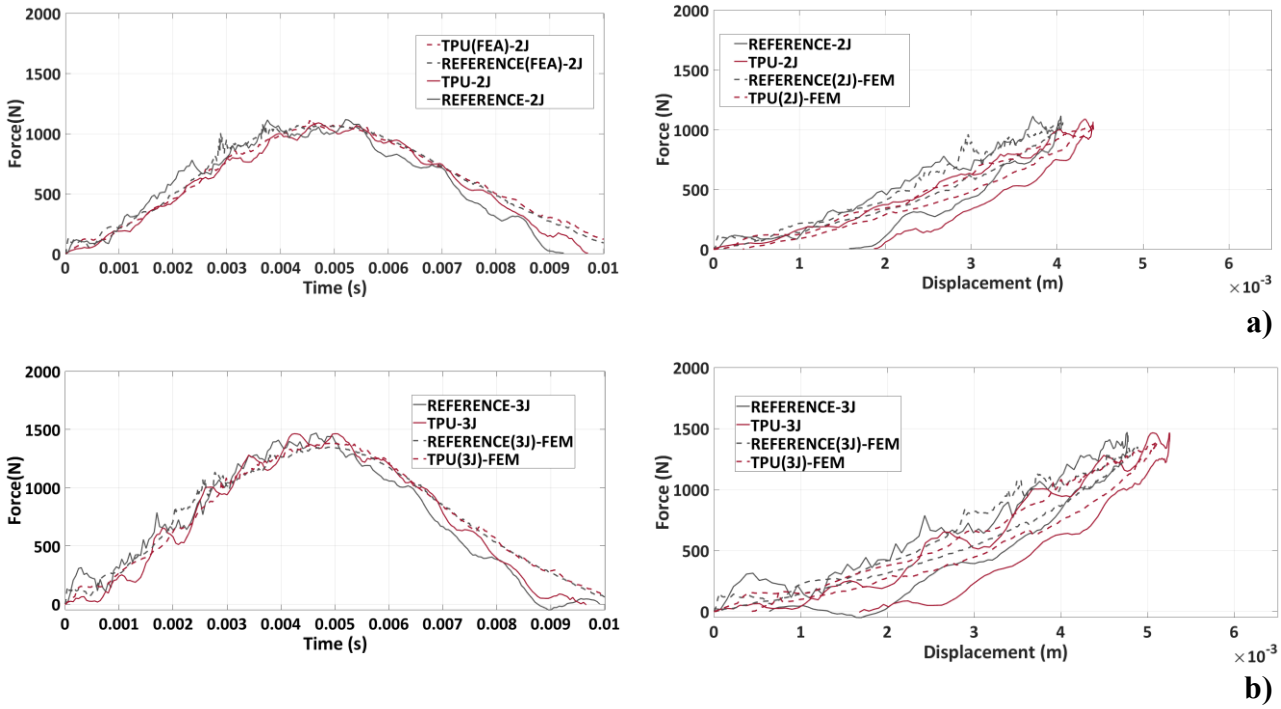

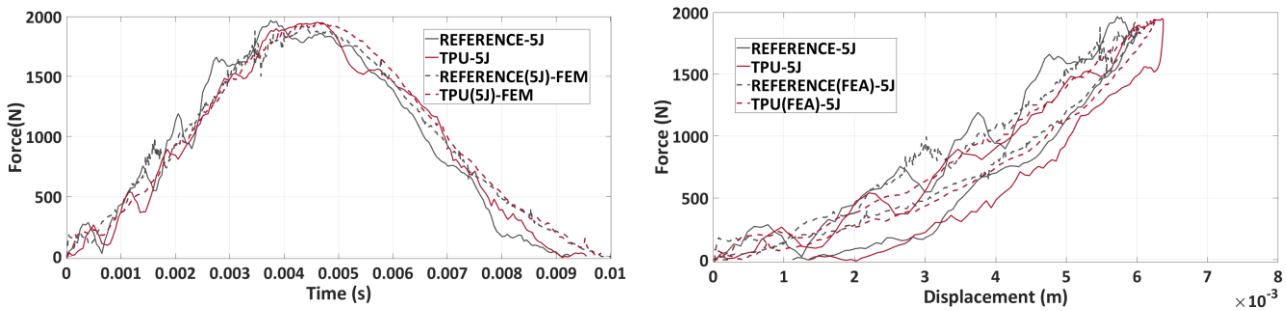

Figure 10- Impact results curves obtained from impact tests on Control and TPU samples for different levels of energy: a) 2J, b) 3J and c) 5J). Force-time and Force-Displacement curves reported.

The extent of the internal damage was evaluated using Phased array scans (Figure 11) from which a statistical analysis was carried out to demonstrate the consistency of damage extension results. Similarly, to understand the typology and topology of the damage inside the laminate's structure and to assist Phased-Array results, CT-scan images were examined. (Figure 12)

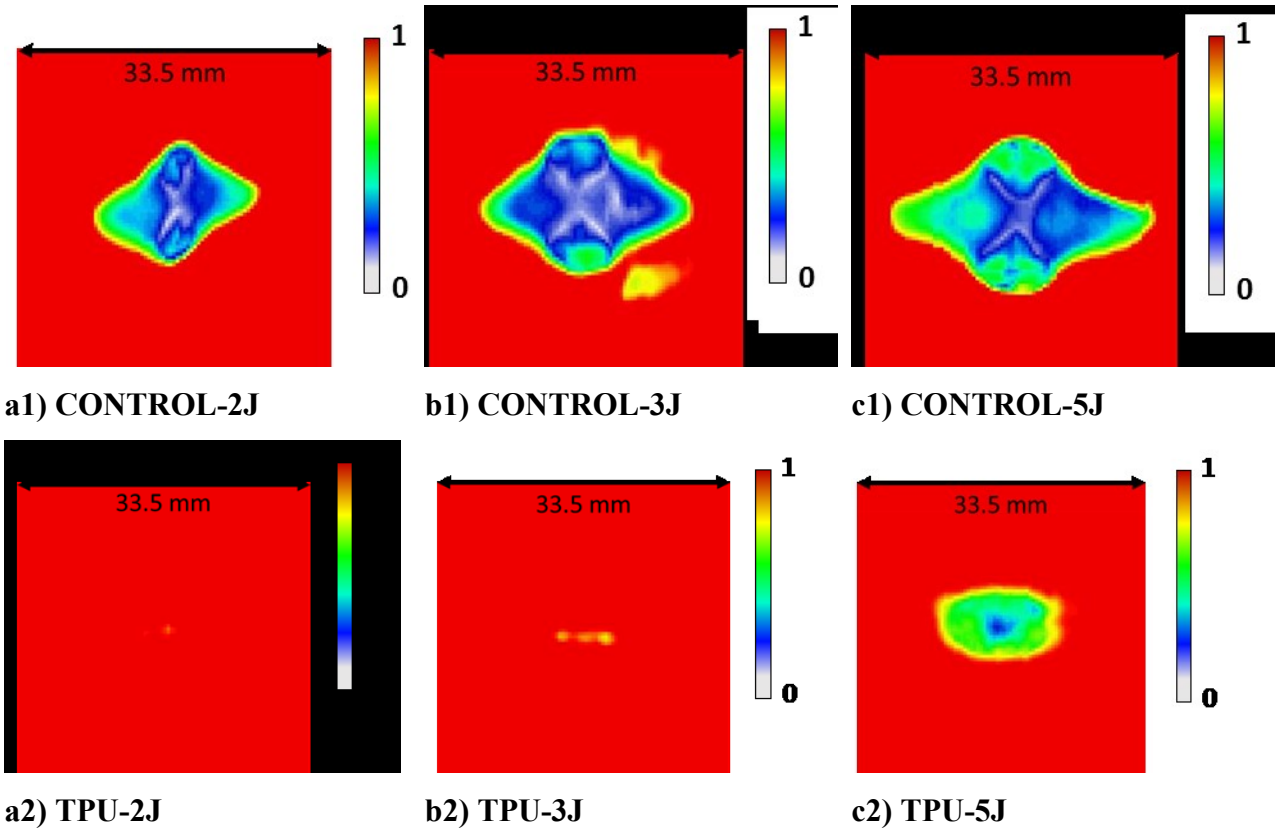

Figure 11-Phased-Array scans from the impacted samples: a1,b1,c1) control samples impacted at 2J,3J and 5J, , b1,b2,c2) TPU-coated samples impacted at 2J,3J and 5J. Images are collected from the external surface, far from the impacted one. The colour scale represents the normalised amplitude.

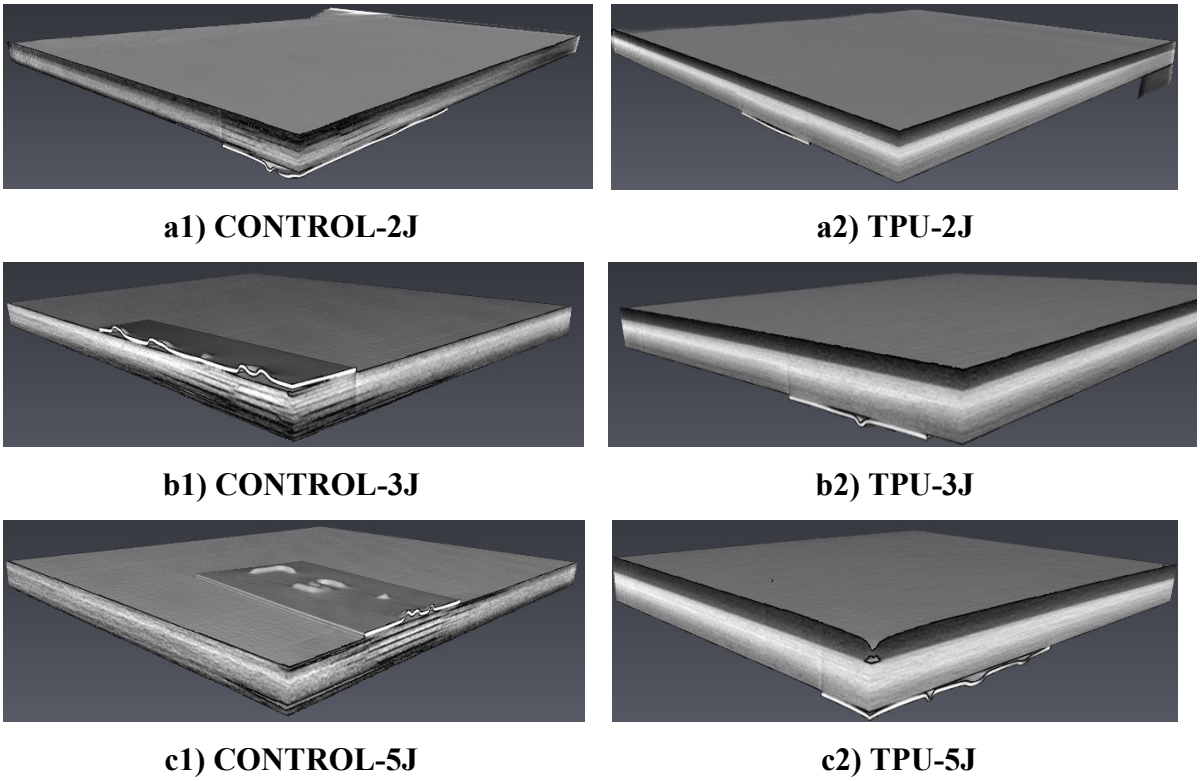

426 **Figure 12- CT scan damage detection technique from the impacted samples: a1,b1,c1) control samples impacted**
427 **at 2J,3J and 5J, , b1,b2,c2) TPU-coated samples impacted at 2J,3J and 5J.**

428

429 Statistical data with mean values and standard deviations for each energy level and configuration are
430 reported and compared in Table 3 and Figure 13.

REFERENCE					
Energy (J)	**Time of Contact (ms)**	**Peak Force (N)**	**Max Displacement (mm)**	**Absorbed Energy (J)**	**Delaminated Area (mm^2)**
2	***9.34 ± 0.188***	***1083 ± 18***	***4.05 ± 0.10***	***0.95 ± 0.02***	***234.2 ± 24.1***
3	***9.07 ± 0.33***	***1420 ± 20***	***4.78 ± 0.26***	***1.32 ± 0.06***	***350.9 ± 2.6***
5	***8.78 ± 0.33***	***1895 ± 57***	***5.93 ± 0.26***	***2.21 ± 0.20***	***485.5 ± 67.9***
TPU					
Energy (J)	**Time of Contact (ms)**	**Peak Force (N)**	**Max Displacement (mm)**	**Absorbed Energy (J)**	**Delaminated Area (mm^2)**
2	***10.12 ± 0.22***	***1103 ± 42***	***4.56 ± 0.21***	***0.88 ± 0.07***	***0***
3	***9.58± 0.06***	***1421 ± 13***	***5.04 ± 0.32***	***1.33 ± 0.09***	***0***
5	***9.14 ± 0.20***	***1976 ± 43***	***6.22 ± 0.29***	***2.19 ± 0.09***	***157.4 ± 20.5***

Table 3-Statistical data from impact campaign. 2J, 3J and 5J are the impact energies and the impact parameters of Time of Contact, Peak Force, Maximum Displacement, Absorbed Energy and Delaminated area are reported.

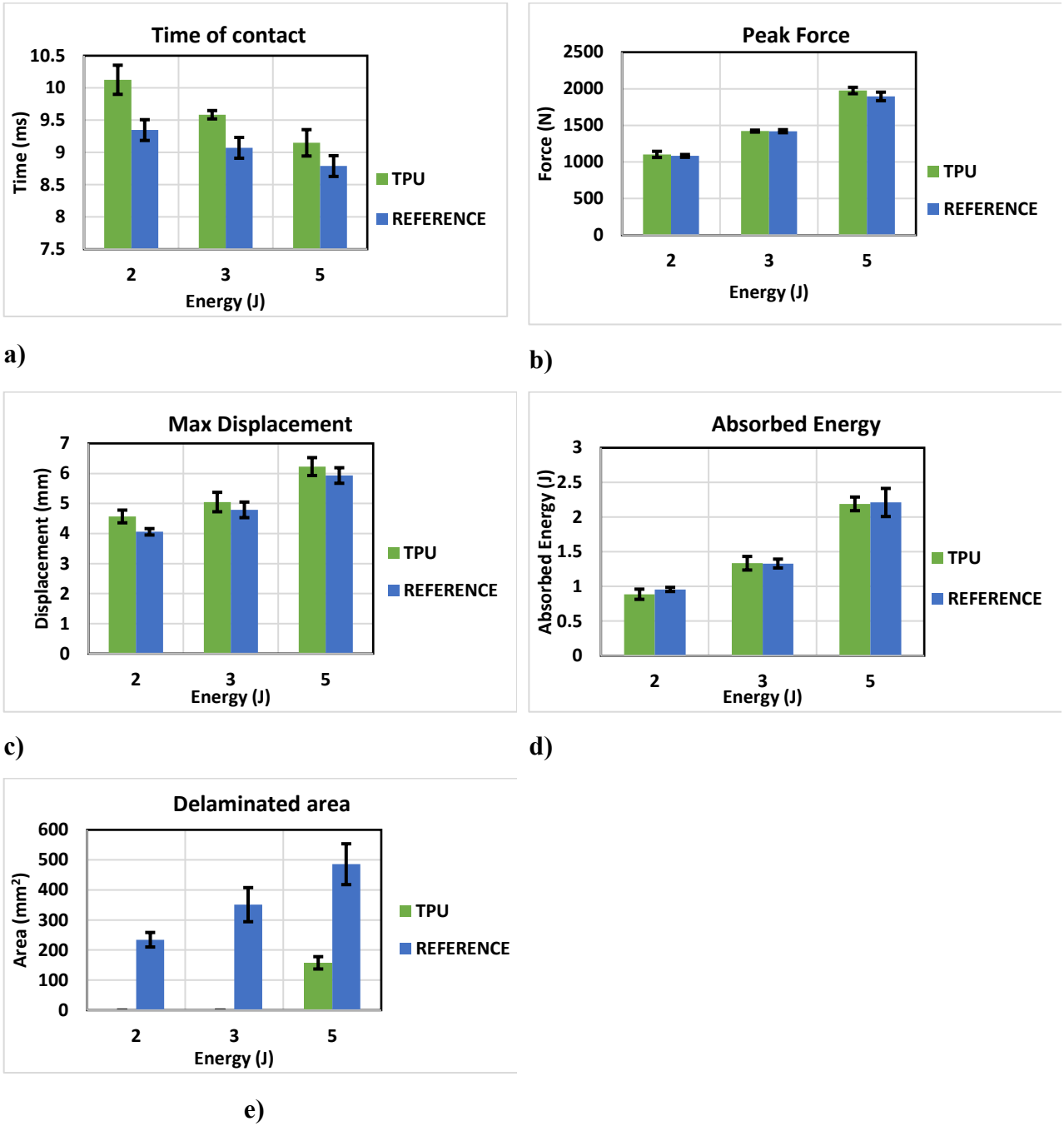

Figure 13- Statistical data charts on impacted data for 2J, 3J and 5J impacts. Mean values for each impact parameters and respective standard deviations are reported in the column chart for control and TPU sets: a) time of contact, b) maximum contact force, c) maximum displacement, d) absorbed energy and e) damaged area extension measured from C-scan images. TPU samples have no structural damage within the CFRP portion and the reported values correspond to the TPU-CFRP interface separation.

As predicted in literature (37), the impact behaviour of both configurations changes according to the impact energy. In particular, for TPU/CFRP samples, maximum displacement and time of contact (in comparison with uncoated samples) increase by +8.34% and +12.58% for 2J, +5.66% and +5.44%

for 3J and, +4.10% and 5.01% for 5J, (see Figure 13.c and Figure 13.a), reporting that the increase in displacement between TPU coated and control samples tends to decrease for higher energetic impacts due to the viscoelastic effect of TPU layer (38). The presence of TPU has reduced influence on force peak values (Figure 13.b) with minimal variations in terms of impact response for the different energy levels (see Figure 10). The percentage variation in comparison with the reference is +1.85% for 2J, +0.08% for 3J and +4.26% for 5J.

Another important results is shown from Figure 13.d, where a similar absorbed energy is reported for both tested configurations (see Figure 13.e), suggesting that the presence of the TPU coating enables different energy absorption mechanisms. As a consequence, it is important to correlate the information obtained with the LVIs tests with the internal integrity status of post-impact samples. Phased-Array images of control samples (Figure 11) indicate widespread damaged areas with damage extension increasing with impact energy. In contrast, TPU/CFRP samples show no signs of defects within the laminate, with the exception of the samples impacted at 5J, where a small damage can be seen in correspondence with the indentation point area. The variations in terms of damaged areas between TPU-coated and traditional CFRP samples are -100% for 2J (undamaged), -100% for 3J (undamaged) and -67.5% for 5J. CT scan images of the control samples (Figure 12) show wide damaged areas that can be clearly identified as a typical reversed pine-tree propagation shape characteristic of matrix failure, whose severity and extension increase with the increase of impact energy, confirming the results shown for Phased-array images. On the contrary, CT scan images of TPU-coated samples show no signs of damage in the entire body of laminate for all impact energies, in apparent contrast with what observed with the Phased-Array scans for the 5J samples (Figure 11.c2). The difference between the outputs of the two tests was found to be due to the presence of a small area within the TPU layer showing signs of interface separation between TPU and CFRP that was indistinguishable from a structural damage from the Phased-Array images. Consequently, TPU coated samples impacted at 5J do not present any sign of structural damage in the CFRP portion since the damaged area detected in the Phased-Array images corresponds to the TPU interface separation.

By comparing the experimental results with the output of the numerical model, it is possible to observe that the model is able to predict the damage-suppression ability of the TPU coating, as reported in the comparison graphs in Figure 10. In particular, the numerical curves for traditional CFRP laminate show load drops similar to the ones observed experimentally (around 3ms for 2 and 3 J, and around 3ms and 4.5ms for 5J), while numerical simulation of the TPU-coated samples show no damage, also confirming the experimental results. An error of +2% and -0.7% for 2J for uncoated laminates and +8% and +3% for the TPU/CFRP is found in terms of maximum contact force and maximum displacement between experimental and numerical results, showing a good accuracy in

predicting the impact output data for both traditional and TPU/CFRP. Similarly, considering 3J impacts, the overall for maximum contact force and maximum displacement is around the same values detected for the 2J impact case with +5% and -0.2% respectively for the reference samples and +2% and -0.1% for the TPU/CFRP ones. 5J impact case, as well, shows differences in the terms of maximum force and maximum displacement similar to the two previous cases, reporting -1% and -4% for the reference configuration and +1% and +0.3% for the hybrid case. Thus, the results show a good correlation between experimental data and the numerical model for values of stiffness, maximum displacement and maximum contact force, even if the force-displacement descendent curve portion presents a slight mismatch. These small variations can be the result of the formation of defects during the cure process that affect the numerical data for mechanical properties and the elastic energy release during the unloading phase of the impact event.

In order to explain the different behaviour of the TPU-coated CFRP, it is important to analyse the different mechanisms utilised to store or absorb energy by estimating the energy transfer from the impacting mass to the sample during the impact event (34,35,36). In general, for LVI impacts where no visible damage is reported, a total kinetic energy transfer (E_{total}) takes place from the impactor's tip to the sample in correspondence with the contact point, and the energy is distributed into the laminate with different forms. One such form is the elastic energy contribution ($E_{elastic}$), which represents the ability of the material to store energy via non-permanent geometrical deformation. This energy is transferred back to the penetrator after maximum displacement of the plate is reached. Another form is the energy absorbed ($E_{absorbed}$) by the impacted object (39,41,42). Therefore, for the energy conservation balance it is possible to write:

$$E_{total} = E_{elastic} + E_{absorbed} \quad (8)$$

$E_{absorbed}$ can be further divided into three different contributions: E_{damage}, representing the energy required to generate damage inside the structure (e.g. fibre failure, matrix failure and delamination), $E_{viscous}$ that is the energy absorbed via viscoelastic mechanisms (43) and $E_{dissipation}$ which encompasses all other dissipation modes including heat, inelastic behaviour of components and all non-linear behaviours. Thus, the equation can be written as:

$$E_{total} = E_{elastic} + E_{damage} + E_{viscous} + E_{dissipation} \quad (9)$$

Considering the layered nature of CFRP, (44), in traditional laminates damage generation is the main cause of energy dissipation, due to the creation of new surfaces between two adjacent plies at different fibre orientations (i.e. delamination). For this reason, a notable amount of energy is absorbed in a laminated system and the E_{damage} term represents the highest contribution in equation (9).

In contrast, using a TPU layer, an additional damage suppression ability is introduced into the CFRP system due to the high strain at failure and damping ability of the polymer (45).

Indeed, since TPU is characterised by a lower stiffness and higher strain at failure, it is able to increase the global elastic energy threshold that the material can tolerate before damage is generated. As a consequence, a lower amount of energy is found into the E_{damage} term and consequently, less impact energy is dissipated via the creations of defects.

In addition, the hybrid system is able to absorb a larger amount of impact energy via viscoelastic losses of TPU layer. This allows to take into account more energy into the $E_{viscous}$ term and lower the weight of the E_{damage} term, meaning smaller damaged areas generated into the sample.

Therefore, it is possible to conclude that the coupled effects of increased elastic properties and improved damping given by the TPU layer, allow the absorption of all the impact energy via these two components, generating no damaged areas within the laminate's body.

4. Compression-after-Impact (CAI)

In order to confirm the results obtained with the LVIs and the NDT analyses, post-impact samples were subjected to a Compression-After-Impact (CAI) campaign to analyse the residual compressive strength and prove the damage suppression ability of the TPU layer.

4.1. Experimental setup

CAI tests were performed using an Instron Universal Machine 5585 in compressive mode following the standard ISO 19352:2009. A rig of 150mm x 100 mm was used to constrain the sample and guarantee a pure compressive load applied on the sample section. A schematisation of the used rig is reported in Figure 14:

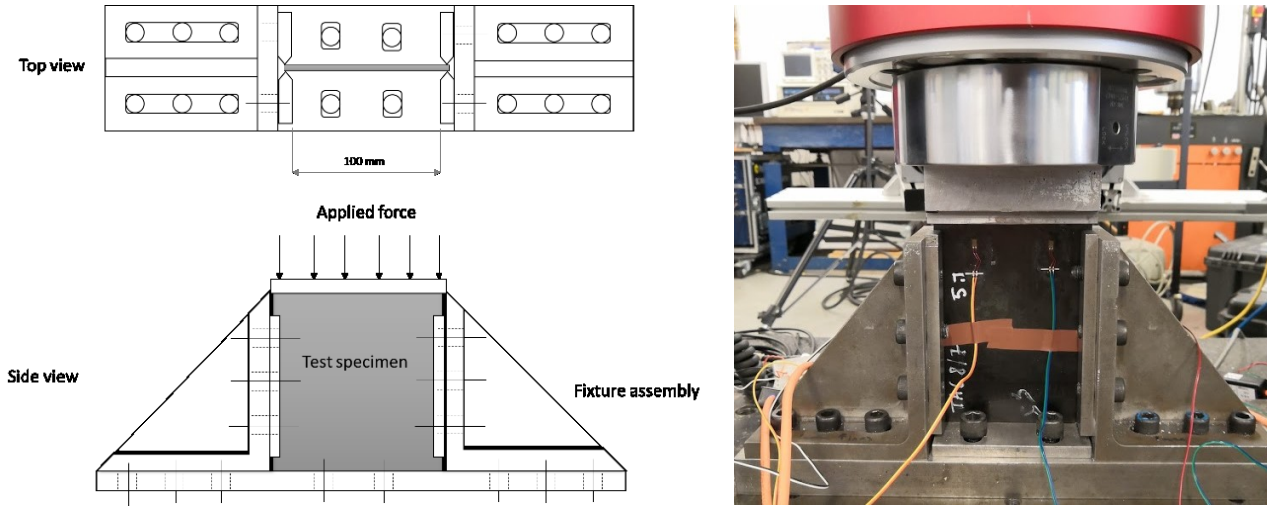

Figure 14-Schematisation of CAI rig assembly

Samples were stabilised at the edges by the fixture without constraining the in-plane transverse deformation. For all tested samples, four strain gauges were used in order to record the applied strain and ensure the parallelism to the lateral supports, flatness and exact positioning of the sample in the rig. During the tests, the force was recorded and elaborated using equation 10 to evaluate the residual compressive strength of each sample. Considering this equation, F_{CAI} is the peak force reached during the compression test while S is the cross-section area as stated in the standard test method.

$$\sigma_{CAI} = \frac{F_{CAI}}{S}. \tag{10}$$

4.2. Results and discussion

CAI results are reported in **Error! Reference source not found.**Figure 15, where output values correspond to the residual compressive strength evaluated considering 100% as an undamaged CFRP structure.

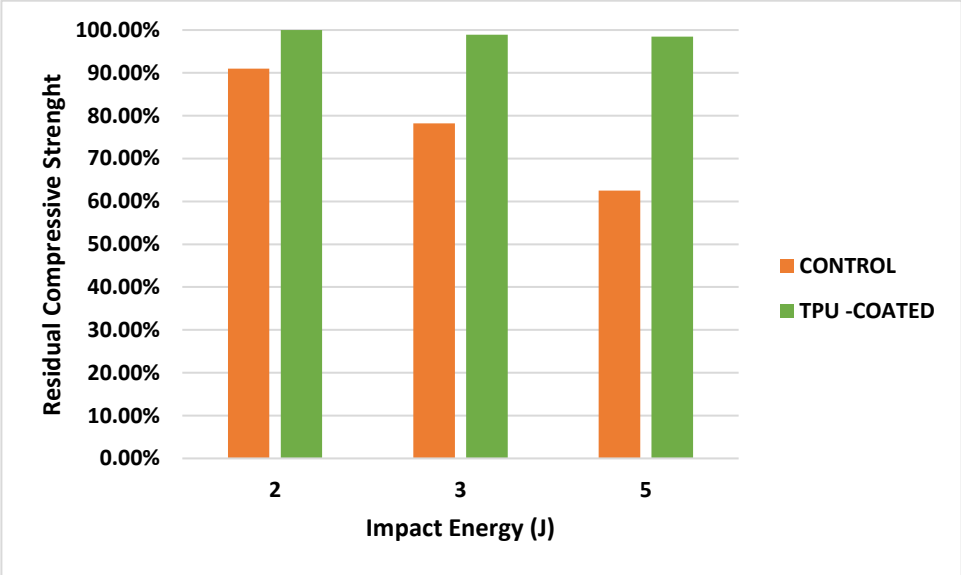

Figure 15- CAI results obtained from the test of samples impacted at 2J, 3J and 5J

Since TPU coated samples showed an asymmetrical geometry (TPU layer on one surface) during CAI failure, a small bending component was observed affecting the recorded compressive strength. This led to an oscillation in the residual compression strength for TPU-coated samples at different impact energies. In order to overcome this issue, TPU layer was carefully removed from the samples prior to the tests ensuring that no damage was created within the laminate during the operation using c-scan analyses.

As it is possible to see from the results, traditional CFRP samples show a significant reduction in terms of residual compressive strength that becomes more dramatic as the impact energy increases

(90.96% for 2J, 78.19% for 3J and 62.54% for 5J). TPU samples instead, show higher in-plane residual compressive properties due to the absence of damaged areas in the laminate body, confirming what observed from the previous tests.

5. Conclusions

The principal aim of this work was to investigate the improvement of the impact properties derived from the application of a layer of Thermoplastic Polyurethane blend as coating layer on the impact surface of CFRP laminates. This superficial layer was applied on the samples' surface during the lamination sequence prior to the curing process, using a "one-step" manufacturing process aimed at reducing costs and time in comparison with conventional coating procedures. An extensive study was carried out using Differential Scanning Calorimetry (DSC) and Dynamic Mechanical Analysis (DMA) to determine the optimal cure parameters for autoclave curing in function of the thermal properties of the polymer and the operative conditions in railways. Results showed TPU glass transaction at -33°C and mechanical properties degradation at 150°C in range of frequency between 1 and 80Hz that overestimates the real operative conditions of the material in railways. Damping tests were performed showing an increment of 113% and 387% in logarithm decrement for the TPU/CFRP manufactured with the "one-step" process in comparison with TPU glued on CFRP and traditional uncoated CFRP. An impact campaign was then carried out and the results indicated that traditional CFRP laminates show large internal damaged areas that become larger for higher impacts, while no sign of damage was found in the TPU coated laminates. This is attributed to the presence of TPU capable of storing elastic energy and dissipate higher amount of impact energy via viscoelastic losses, with no measurable damage (i.e. cracks and delamination). This results was confirmed by analysing the residual compressive strength of traditional and TPU-coated laminates, showing no variation in residual mechanical properties for TPU-coated CFRP since no damage was generated during LVI event. In contrast, traditional CFRP laminates showed a significant variation in residual strength (90% for 2J, 78% for 3J and 62% for 5J) in function of impact energy due to delamination. A numerical model was then developed to support the optimisation process of the TPU-coated CFRP for designing future advanced structural components where this material will be used. A good correlation between experimental and numerical results was found with a maximum error of 8% between experimental and numerical data, demonstrating that the developed numerical model is an excellent tool to predict the mechanical response of TPU/CFRP laminates.

In conclusion, the introduction of TPU as an additional reinforcement layer for damage suppression makes hybrid TPU/CFRP laminates a promising candidate for the development of a new generation of lightweight railways vehicles, able to withstand flying ballast-like events without the generation of BVIDs, enhancing safety and reliability of the entire rolling stock.

Funding

The author(s) disclosed receipt of the following financial support for the research, authorship, and/or publication of this article: This paper has been funded by the EXTREME project of the European Union's Horizon 2020 research and innovation programme under Grant Agreement No. 636549.

References

1. UNI EN 12663. 2010;
2. Standard E. EUROPÄISCHE NORM Railway applications - Crashworthiness requirements for railway vehicle bodies. 2005;
3. Group RD. Rail Delivery Group Charges and Incentives User Guide June 2014. 2014;(June).
4. Tech EE. Energy Efficiency Strategies for Rolling Stock and Train Operation. Technical Report; 2005.
5. Mair RI. Fibre Reinforced Polymers-From Aerospace to Infrastructure. Society of Manufacturing Engineers; 2000.
6. Vlot A. Glare: history of the development of a new aircraft material. Vol. 1, Kluwer Academic Publishers. 2001. 222 p.
7. Gunnink JW, Vlot A, De Vries TJ, Van Der Hoeven W. Glare technology development 1997-2000. Appl Compos Mater. 2002;9(4):201–19.
8. Koenig J, Friedrich IH. Integral consideration of the lightweight design for railway vehicles. InYoung researchers seminar 2011.
9. Goo JS, Kim JS, Shin KB. Evaluation of structural integrity after ballast-flying impact damage of a GFRP lightweight bogie frame for railway vehicles. J Mech Sci Technol. 2015;29(6):2349–56.
10. Grasso M, Gallone A, Genovese A, Macera L, Penta F, Pucillo G, Strano S. Composite Material Design for Rail Vehicle Innovative Lightweight Components. InProceedings of the World Congress on Engineering 2015 ;2: 1-3.
11. Heller P, Korinek J, Triska L. HYBRID BODY OF UNDERGROUND RAILWAY CAR: PATH TOWARDS REDUCED WEIGHT OF RAIL VEHICLES. MM Sci J [Internet]. 2015;665–9. Available from: http://www.mmscience.eu/content/MM_Science_201516.pdf
12. SiebelT. C, G Rail unveils world's first CFRP rail vehicle, [Internet] ,USA, Composite World, [2018/9/19; 2019/5/31]. Available from:https://www.compositesworld.com/news/cg-rail-unveils-worlds-first-cfrp-rail-vehicle
13. Abrate S. Impact on Laminated Composite Materials. Appl Mech Rev [Internet]. 1991;44(4):155. Available from: http://appliedmechanicsreviews.asmedigitalcollection.asme.org/article.aspx?articleid=1394347
14. Onder A, Oneill C, Robinson M. Flying Ballast Resistance for Composite Materials in Railway Vehicle Carbody Shells. In: Transportation Research Procedia. 2016. p. 595–604.
15. Cantwell WJ, Morton J. Impact resistance of composite materials. A review. Composites [Internet]. 1991;22(5):347–62. Available from: http://dx.doi.org/10.1016/0010-4361(91)90549-V
16. Cartié DDR, Irving PE. Effect of resin and fibre properties on impact and compression after impact performance of CFRP. Compos - Part A Appl Sci Manuf. 2002;33(4):483–93.
17. Wang S-X, Wu L-Z, Ma L. Low-velocity impact and residual tensile strength analysis to carbon fiber composite laminates. Mater Des [Internet]. 2010;31(1):118–25. Available from: http://linkinghub.elsevier.com/retrieve/pii/S0261306909003446
18. Riccio A, Russo A, Sellitto A, Raimondo A. Development and application of a numerical procedure for the simulation of the "Fibre Bridging" phenomenon in composite structures.

Compos Struct. 2017;

19. Riccio A, Linde P, Raimondo A, Buompane A, Sellitto A. On the use of selective stitching in stiffened composite panels to prevent skin-stringer debonding. Compos Part B Eng. 2017;
20. Rechak S, Sun CT. Optimal Use of Adhesive Layers in Reducing Impact Damage in Composite Laminates. Compos Struct 4 [Internet]. 1987;9(6):18–31. Available from: http://www.springerlink.com/index/10.1007/978-94-009-3457-3_2
21. Siegfried M, Tola C, Claes M, Lomov S V., Verpoest I, Gorbatikh L. Impact and residual after impact properties of carbon fiber/epoxy composites modified with carbon nanotubes. Compos Struct. 2014;111(1):488–96.
22. RuggeriR, Martin RE, and Mccorkle LS. Impact behavior of composite fan blade leading edge subcomponent with thermoplastic polyurethane interleave. NASA, 2015, pp. 19–24. In: 20th International Conference on Composite Materials; 19-24 Jul. 2015; Copenhagen; Denmark.
23. Martone A, Antonucci V, Zarrelli M, Giordano M. A simplified approach to model damping behaviour of interleaved carbon fibre laminates. Compos Part B Eng. 2016;97:103–10.
24. Russo P, Langella A, Papa I, Simeoli G, Lopresto V. Low-velocity Impact and Flexural Properties of Thermoplastic Polyurethane/Woven Glass Fabric Composite Laminates. In: Procedia Engineering. 2016. p. 190–6.
25. Pichaiyut S, Nakason C, Vennemann N. Thermoplastic elastomers-based natural rubber and thermoplastic polyurethane blends. Iran Polym J (English Ed. 2012;21(1):65–79.
26. Rathod VT, Kumar JS, Jain A. Polymer and ceramic nanocomposites for aerospace applications. Appl Nanosci. 2017;
27. Lucchini UK, Axle Surface Coatings, [Internet], UK, Institution of Mechanical Engineers, [2018/4; 2019/5/31]. Available from: http://files.imeche.org/events/downloads/S1486/Axle%20Coatings.%20Sean%20Barson.pdf;
28. Frick A, Rochman A. Characterization of TPU-elastomers by thermal analysis (DSC). Polym Test. 2004;23(4):413–7.
29. ISO 6721-11:2012 Plastics — Determination of dynamic mechanical properties —.
30. EN 50125 -. 2008;
31. REFRESCO, Damages scenarios, Deliverable 7.2, [Internet] ,EU, UNIFE, [2014/12; 2019/5/31]. Available from: http://www.refresco-project.eu/wp-content/uploads/2015/02/D7.2_Damage_Scenarios.pdf
32. Pinho ST, Iannucci L, Robinson P. Physically based failure models and criteria for laminated fibre-reinforced composites with emphasis on fibre kinking. Part II: FE implementation. Compos Part A Appl Sci Manuf. 2006;
33. Manual, LS-DYNA Keyword User'S. "vol. II." Livermore Software Technology Corporation (LSTC) (2013);
34. Hallquist JO. LS-DYNA keyword user's manual. Livermore Softw Technol Corp. 2007;970:299–800.
35. Thota NM, Epaarachchi JA, Lau KT. Evaluation of the blunt thoracic trauma due to baseball impacts–review of the Blunt Criterion. 2014;
36. Smith L, Nevins D, Dat NT, Fua P. Measuring the accuracy of softball impact simulations. Sport Eng. 2016 Dec;19(4):265–72.
37. Abrate S. Impact on Composite Structures. 2005. 304 p.

38. Qi HJ, Boyce MC. Stress-strain behavior of thermoplastic polyurethanes. Mech Mater. 2005;

39. Delfosse D, Poursartip A. Energy-based approach to impact damage in CFRP laminates. Compos Part A Appl Sci Manuf. 1997;28(7):647–55.

40. Shyr TW, Pan YH. Impact resistance and damage characteristics of composite laminates. Compos Struct. 2003;62(2):193–203.

41. Williams K V., Vaziri R. Application of a damage mechanics model for predicting the impact response of composite materials. Comput Struct [Internet]. 2001;79(10):997–1011. Available from: http://ac.els-cdn.com/S0045794900002005/1-s2.0-S0045794900002005-main.pdf?_tid=dbd0ea4a-42cc-11e5-aa7b-00000aacb362&acdnat=1439588513_b6c79eda6172dc2053acb31fc1cc79de

42. Shyr T-W, Pan Y-H. Impact resistance and damage characteristics of composite laminates. Compos Struct [Internet]. 2003;62(2):193–203. Available from: http://linkinghub.elsevier.com/retrieve/pii/S0263822303001144

43. Jones DIG. Handbook of Viscoelastic Vibration Damping. John Wiley & Sons Ltd, editor. 2001.

44. Wisnom MR. The role of delamination in failure of fibre-reinforced composites. Philos Trans R Soc A Math Phys Eng Sci [Internet]. 2012;370(1965):1850–70. Available from: http://rsta.royalsocietypublishing.org/cgi/doi/10.1098/rsta.2011.0441

45. Nakamura M, Aoki Y, Enna G, Oguro K, Wada H. Polyurethane damping material. J Elastomers Plast. 2015;47(6):515–22.